[^{18}F]SuFEx Click Chemistry Enabled Ultrafast Late-stage Radiosynthesis

Qinheng Zheng[1,5], Hongtao Xu[2,5], Hua Wang[1,3], Wen-Ge Han Du[4], Nan Wang[2], Huan Xiong[2], Yuang Gu[2], Louis Noodleman[4], K. Barry Sharpless[1*], Guang Yang[2*] and Peng Wu[3*]

[1]Department of Chemistry, The Scripps Research Institute, La Jolla, CA 94037, United States. [2]Shanghai Institute of Advanced Immunochemical Studies (SIAIS), ShanghaiTech University, Shanghai 201210, China. [3]Department of Molecular Medicine, The Scripps Research Institute, La Jolla, CA 92037, United States. [4]Department of Integrative Structural and Computational Biology, The Scripps Research Institute, La Jolla, CA 92037, United States. [5]These authors contributed equally: Qinheng Zheng, Hongtao Xu. *E-mail: pengwu@scripps.edu (P.W.), sharples@scripps.edu (K.B.S.), yangguang@shanghaitech.edu.cn (G.Y.).

Abstract:

The lack of efficient [^{18}F]fluorination processes and target-specific organofluorine chemotypes remains the major challenge of fluorine-18 positron emission tomography (PET). We report here an ultrafast isotopic exchange method for the radiosynthesis of novel PET agent aryl [^{18}F]fluorosulfate enabled by the emerging sulfur fluoride exchange (SuFEx) click chemistry. The method has been applied to the fully-automated ^{18}F-radiolabeling of twenty-five structurally and functionally diverse aryl fluorosulfates with excellent radiochemical yield (83–100%, median 98%) and high molar activity (281 GBq μmol^{-1}) at room temperature in 30 seconds. The purification of radiotracers requires no time-consuming HPLC, but rather a simple cartridge filtration. We further demonstrate the imaging application of a rationally designed poly(ADP-ribose) polymerase 1 (PARP1)-targeting aryl [^{18}F]fluorosulfate by probing subcutaneous tumors *in vivo*.

The non-invasive molecular imaging technique – positron emission tomography (PET), especially that based on the radionuclide fluorine-18, is widely used for tracking biological processes *in vivo*[1-6]. PET imaging has found successful clinical applications in the diagnosis of malignant tumor or neurodegenerative diseases and the efficacy evaluation of therapeutic treatment. Ever-growing fluorination methodologies over the past decades with a focus on the formation of C–^{18}F bonds sparked the expansion of ^{18}F-based toolbox of radiotracers[7-11].

Despite a few state-of-the-art methods[12-19] reported to date, harsh reaction conditions and laborious purification that a common C–^{18}F forming process requires have, nevertheless, significantly limited the substrate scope and clinical utility. [^{18}F]Fluorodeoxyglucose (FDG), an agent developed half a century ago to map glucose metabolism[20], remains the predominant shareholder of the clinically used PET radiopharmaceuticals. As noted by Fowler, radiochemists are *working against time*[1] due to the short half-life of fluorine-18 (109.77 min). With these challenges[21], an ideal ^{18}F-radiosynthesis should be: 1) a rapid, mild, and clean ^{18}F-incorporation in the final step of a synthetic sequence; 2) effective for a diverse spectrum of bioactive organofluorine compounds with reasonable *in vivo* stability; and 3) compatible with automation. These stringent criteria mirror those set for click chemistry[22].

We envisioned[23] that the newly developed sulfur(VI) fluoride exchange (SuFEx) reactions[24] would naturally bridge click chemistry and ^{18}F-radiosynthesis. As demonstrated in the first SuFEx manifesto[23] and subsequent reports, aryl fluorosulfate ($ArOSO_2F$) tops the rank of the stability hierarchy of the most demure electrophiles (*Cf.* sulfonyl fluoride, RSO_2F). This functional group may only become reactive in the presence of a proper catalyst in organic solvents or upon encountering a specific protein partner, if any, that possess both a nucleophilic amino acid side chain and juxtaposed side chains, e.g. arginine to provide hydrogen bonding networks for the extraction and transport of the departing fluoride in the binding site. In most cases, nevertheless, aryl fluorosulfates simply remain intact in aqueous solutions near neutral conditions in the presence of nucleophilic amino acids, e.g. lysine, serine, threonine, and

tyrosine (**Fig. 1b**), and even in an entire proteome[24]. Its compatibility with most common medicinal chemistry transformations (**Fig. 1b**) has also led to its use as a protecting group[25]. Importantly, our proof-of-principle pharmacokinetic evaluations have provided strong evidence of the inertness of several bioactive aryl fluorosulfates *in vivo*[25,26].

On the other hand, one can certainly imagine the possibility of an isotopic exchange event in which the ^{18}F-enriched fluoride anion enables its own nucleophilic displacement of the other fluorine atom of an aryl fluorosulfate[27]. This interchange process may actually be much less energy-demanding than a typical SuFEx reaction with amine or alcohol nucleophiles—the extraneous fluoride anion *per se* compensates the stringent requirements in the latter scenario for the stabilization or solvation of the departing fluoride from an S^{VI}–F site. Significantly, compared to the traditional S_N2-based C–F formation SuFEx with F^- might engage the 3d-orbital of S^{VI}, rendering a much lower kinetic barrier[28-33]. Thus, we hypothesize that such a process may take place facilely at room temperature. Given the inertness of many aryl fluorosulfates under physiological conditions, such ^{18}F-labeled aryl fluorosulfates may serve as ideal probes for PET imaging. Here we report the development of an ultrafast ^{18}F-radiolabeling process of preparing aryl fluorosulfate-based probes and their application to PET imaging based on the above principles.

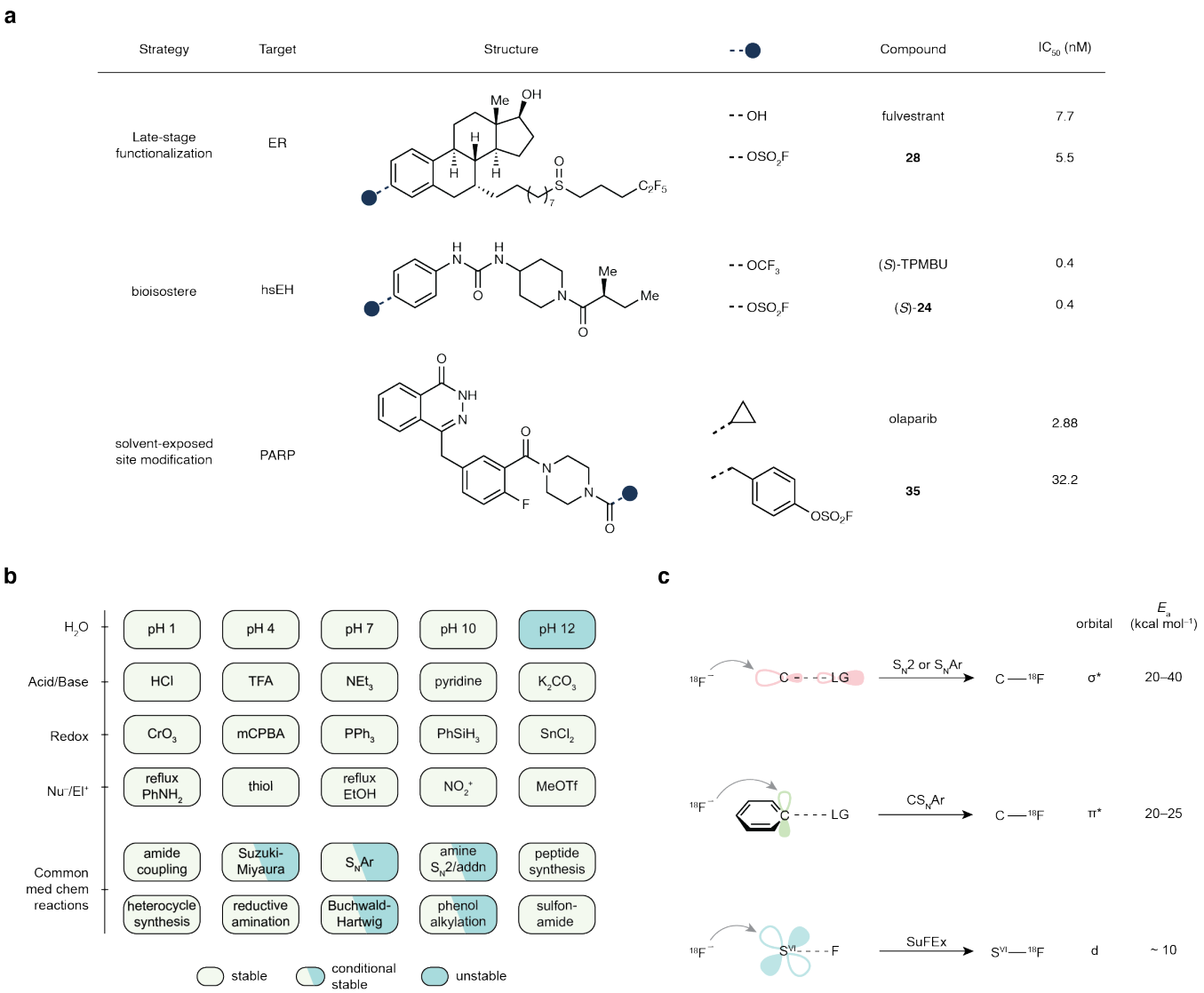

Fig. 1 | Unique properties of aryl fluorosulfates qualify them as potential radiopharmacophore. a, *In vivo* validated non-covalent fluorosulfate inhibitors and strategies for their discovery or rational design. ER, estrogen receptor. hsEH, human soluble epoxide hydrolase. (*S*)-TPMBU, (*S*)-1-(1-(2-methylbutanoyl)piperidin-4-yl)-3-(4-(trifluoromethoxy)phenyl)urea. PARP, poly(ADP-ribose) polymerase. **b**, Matrix showcasing fluorosulfate's broad window of stability under the chemical stress of various conditions including the most used reactions in medicinal chemistry[26]. "Stable" denotes less than 10% decomposition after 2 h incubation under the indicated condition. "Conditional stable" denotes the stability has a case-by-case dependence on the substrate. "Unstable" denotes significant (> 10%)

decomposition after 2 h incubation. TFA, trifluoroacetic acid. mCPBA, 3-chloroperoxybenzoic acid. **c,** Empirical orbital analysis of the three strategies for nucleophilic ^{18}F-incorporation and respective estimated[17,27] activation energies (E_a).

Results

Computational evaluation of sulfur fluoride exchange between phenyl fluorosulfate and anionic fluoride. Computation by density functional theory (DFT) within the conductor like screening (COSMO) solvation model with the dielectric constant of acetonitrile (ε = 18.5) estimated a low barrier for the exchange between phenyl fluorosulfate (**1**) and anionic fluoride (**Fig. 2a**, asterisk for clarity), $\Delta E^{\ddagger}$ = 8.8 kcal mol^{-1} ($\Delta G^{\ddagger}$ = 10.5 kcal mol^{-1}). A pentacoordinated "ate"-complex intermediate formed in the reaction pathway with the two fluorine atoms occupying the two axial vertices (**Fig. 2b**). By contrast, the undesired substitution with amine ($MeNH_2$) possesses a much higher calculated barrier (Supplementary **Fig. S64**, $\Delta G^{\ddagger}$ = 23.2 kcal mol^{-1}, $\Delta\Delta G^{\ddagger}$ = 12.7 kcal mol^{-1}), rendering at least 10^9-fold slower kinetics at room temperature.

Investigation of sulfur fluoride exchange between an aryl fluorosulfate and a fluoride salt by NMR. We used the ^{19}F-NMR time-dependent saturation transfer (TDST) experiments[28] to examine the interchange between an aryl fluorosulfate and a fluoride salt in solution. The TDST assay enables the differentiation of the "reactant" (left-hand side, **Fig. 2a**) and the "product" (right-hand side) for kinetic rate measurements. In this bimolecular system, the fluoride salt signal was irradiated for a set of given saturation times (*TS*). If an intermolecular fluoride exchange process takes place, an apparent drop of the aryl fluorosulfate magnetization (ΔM) would be detected due to saturation transfer (**Fig. 2c**).

Toward this end, SuFEx of phenyl fluorosulfate ($PhOSO_2F$, **1**, 0.02 mol L^{-1}) and tetrabutylammonium bifluoride (*n*-$Bu_4N^+FHF^-$, **2**, 0.2 mol L^{-1}, 10 equiv) was evaluated in acetonitrile-*d*3 (MeCN-*d*3). A set of saturation times (TS_i, subscript *i* for *i*th measurement) was applied to the ^{19}F-nuclei

of **2** (–150 ppm relative to $CFCl_3$) and the corresponding magnetizations (M_i) of **1** were recorded. Plotting M_i versus TS_i, an exponential decay trend was indeed observed. The estimated pseudo-first order rate constant (k_{obs}) was solved by Bloch equation with high coefficient of correlation (0.16 s^{-1}, R^2 = 0.99) (**Fig. 2d**). By varying the concentration of **2**, the second-order rate constant of the exchange between **1** and **2** at 298 K was determined, k_{298K} = 0.43 L mol^{-1} s^{-1} (**Fig. 2e**). Next, an estimation of the exchange barrier was obtained by performing TDST-NMR experiments at various temperatures ranging from 278 to 303 K (**Fig. 2f**). From Eyring Equation, a low enthalpy of activation (11.3 kcal mol^{-1}) was derived, suggesting the SuFEx process to be a facile reaction at room temperature. Furthermore, Hammett plot analysis was performed, which yielded a positive slope greater than unity (ρ = 1.56), indicating the emergence of negative charge during the reaction pathway (**Fig. 2g**).

In parallel, we studied several factors that could influence the SuFEx process. Borosilicate glass, of which normal NMR tubes are made, showed no significant inhibition or acceleration when compared to a plastic reaction vessel (Supplementary **Fig. S11**). By contrast, solvent had significant impact on the rate of fluoride exchange. The use of a polar, aprotic solvent, such as *N*-Methyl-2-pyrrolidone (NMP), *N*,*N*-dimethylformamide (DMF), dimethyl sulfoxide (DMSO), or MeCN was found essential for achieving a fast SuFEx process (**Fig. 2h**).

With tetrabutylammonium as the cation, we screened different fluoride anions (**Fig. 2i**). We found that "basic" fluoride is more effective than its derivatives complexed by Brønsted or Lewis acids (**2**–**5**). Tetrabutylammonium fluoride (**6**•$3H_2O$), although in its nucleophilicity-compromised trihydrate form, exhibited the highest exchange rate, which is approximately 50-fold faster than that of **2**. Results from DFT calculation (**Fig. 2b**) also suggested that the "naked" fluoride anion (**6**) is much more active than its bifluoride counterpart (**2**), $\Delta G_{calc}^{\ddagger}$(**6**) = 10.5 kcal mol^{-1} (*Cf.* $\Delta G_{exp}^{\ddagger}$ (**2**) = 17.7 kcal mol^{-1}, $\Delta\Delta G^{\ddagger}$ = 7.2 kcal mol^{-1}).

Subsequently, the structure-activity relationship of counter ions of bifluoride salts were investigated. Finely powdered potassium bifluoride alone did not effect the fluoride exchange in MeCN, albeit its

complexes with 18-crown-6 (**7**) or [2.2.2]-cryptand (**8**) showed moderate exchange rates. In line with our earlier observation that tris(dimethylamino)sulfonium (TAS^+) was a superior cation for SuFEx reactions[29], the same salt (**10**) showed 10-fold increase in exchange rate compared with **2**.

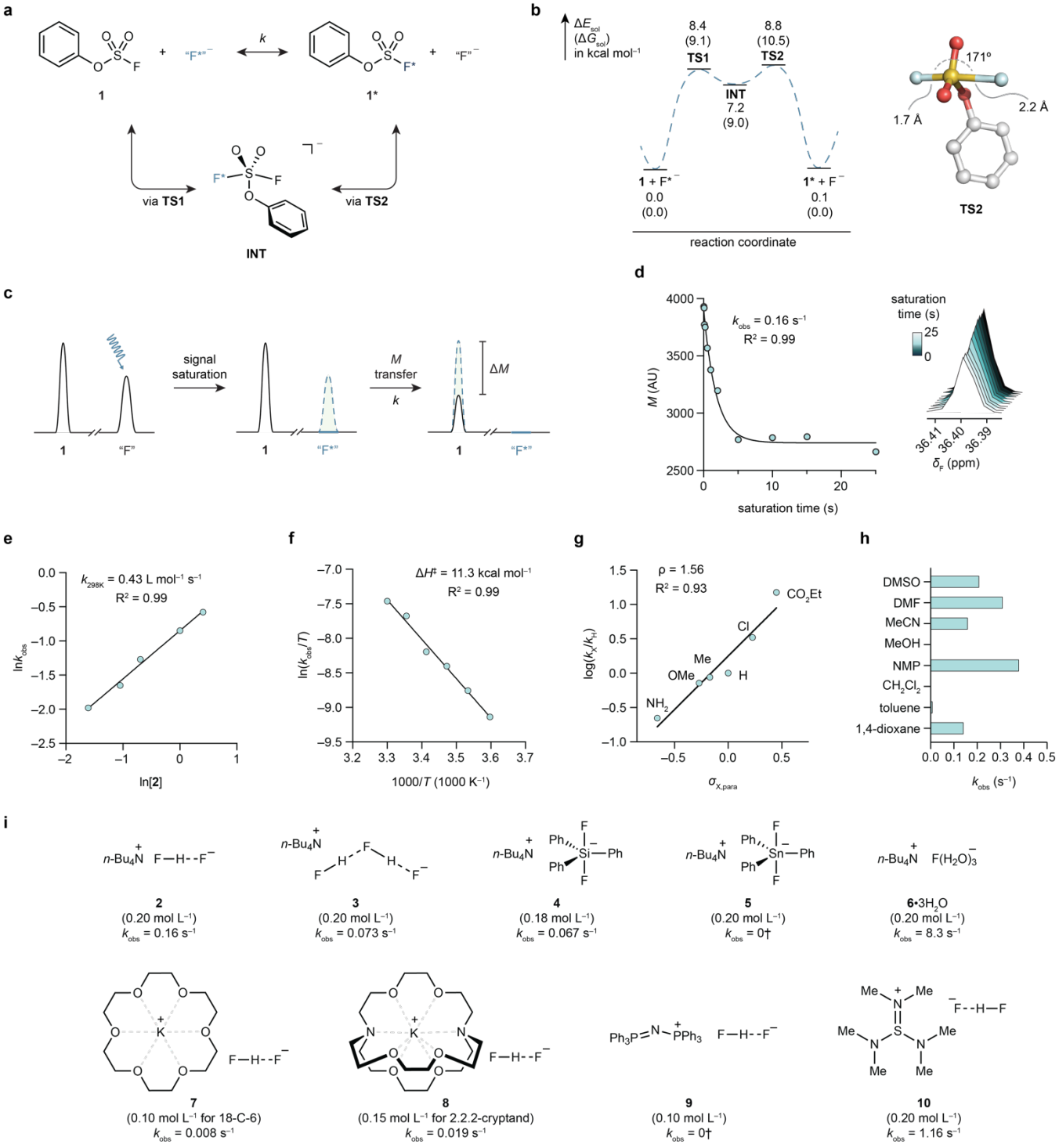

Fig. 2 | Investigation of sulfur fluoride exchange between phenyl fluorosulfate and a fluoride salt. **a**, SuFEx of phenyl fluorosulfate (**1**). "F^-" denotes any nucleophilic fluoride donor, exemplified by those shown below (**h**). **b,** DFT calculated energy profile of a typical SuFEx process in acetonitrile and the optimized geometry of the highest transition state **TS2**. **c,** Schematic illustration of TDST-NMR. **d**, A representative plot of magnetization versus saturation time, and overlapped spectra (right) of the corresponding experiments with saturation time ranging from 0.01 s to 25 s. Conditions: phenyl fluorosulfate (**1**, 0.02 mol L^{-1}), tetrabutylammonium bifluoride (**2**, 0.2 mol L^{-1}), MeCN-*d*3, 298 K. k_{obs} = 0.16 s^{-1} (R^2 = 0.99). **e**, Measurement of the second-order rate of the SuFEx reaction between **1** and **2**, k_{298K} = 0.43 L mol^{-1} s^{-1} (R^2 = 0.99). **f**, Erying plot of the SuFEx reaction between **1** and **2**. The calculated activation enthalpy was determined, $\Delta H^{\ddagger}_{calc}$ = 11.3 kcal mol^{-1} (R^2 = 0.99). **g**, Hammett plot of the SuFEx reactions between **2** and para-X-substituted phenyl fluorosulfates, ρ = 1.56 (R^2 = 0.93). **h**, Solvents effect. **i,** Structure-activity relationship of various fluoride salts (**2**–**10**) on the SuFEx reaction of **1**. †No exchange detected by NMR.

Automated radiosynthesis of aryl [^{18}F]fluorosulfates. With kinetic parameters of [^{19}F]SuFEx between phenyl fluorosulfate and fluoride salts determined, we embarked on the process development of the radioactive [^{18}F]SuFEx. 3-Ethynylphenyl fluorosulfate (**11**) was chosen as the model substrate; potassium fluoride/[2.2.2]-cryptand (**8**) was selected as the [^{18}F]fluoride source for its high elution efficiency and reproducibility. A few rounds of optimization based on the "cold" reaction results yielded a fully automated and highly reproducible method. In a typical experiment, 3-ethynylphenyl fluorosulfate (**11**, 0.1 mg, 0.5 μmol) in MeCN (0.5 mL) was added to azeotropically dried potassium [^{18}F]fluoride (~3.7 GBq) in the presence of [2.2.2]-cryptand (**8**). The complete radiochemical conversion of [^{18}F]F^- was achieved in 30 s at room temperature, showing a single ^{18}F-labeled **11** peak on the crude HPLC traces (**Fig. 3a**,**b**). The radiochemical yield (RCY) based on HPLC[30] was highly reproducible,

99.3 ± 0.6% (*n* = 4), followed by a less-than-one-minute C18-cartridge separation in which 3-ethynylphenyl [^{18}F]fluorosulfate was isolated.

Using this protocol, we successfully synthesized twenty five aryl and heteroaryl [^{18}F]fluorosulfates with excellent RCYs, 83–100% (median 98%, **Fig. 3c**). Bifunctional [^{18}F]fluorosulfate modules (**14**–**20**) covering a wide spectrum of (bio)orthogonally reactive groups could serve as positron-emitting tags for the *in vitro* or *in vivo* functionalization[31] of biomacromolecules with native or preinstalled complementary handles such as alkyne (**14**), amine (**15**), thiol (**16**), hydroxyamine (**17**), *trans*-cyclooctene (**18**,**19**) and azide (**20**). In addition, [^{18}F]SuFEx was applicable to fluorosulfate derivatives of both naturally occurring molecules (**21**, **23**, **25**, **26**) and known phenolic medicines (**22**, **27**, **29**–**34**[32-35]). Importantly, the ^{18}F-isotopologues of *in vivo* validated bioactive fluorosulfates (*S*)-**24**, **28** and **35** (vide infra) were synthesized in the final stage with excellent efficiency and fidelity.

While [^{18}F]SuFEx was rarely interfered by substrates' structures and functionalities, extensive reaction scope assessment revealed the inhibitory effects of acidic groups. Substrates with carboxylic acid (pKa_{exp} = 3.5) and *NH*-tetrazole gave lower RCYs, 50% and 28%, respectively (Supplementary **Figs. S56, S57**). Similarly, excess water was found to be a poison for the fluoride exchange. Only 14% RCY of [^{18}F]**11** was obtained when 50 equiv of water was added (Supplementary **Fig. S27**, Cf. 99% RCY with no water), which was in line with the NMR results (Supplementary **Fig. S15**).

Aryl [^{18}F]fluorosulfate with high molar activity (A_m) was prepared by leveraging the reaction stoichiometry. Incubation of "cold" fluorosulfate **35** with K[^{18}F]F (34.6 GBq, 0.94 Ci) at room temperature for 30 s rendered 98% RCY. The desired [^{18}F]**35** was purified by water quench followed by C18-cartridge separation. Quantitative HPLC analysis of the final product with calibration curve revealed the molar activity 281 GBq μmol^{-1} (decay corrected to end of synthesis), which is about four times as high as the empirical threshold (74 GBq μmol^{-1})[6] for a clinically useful radiotracer.

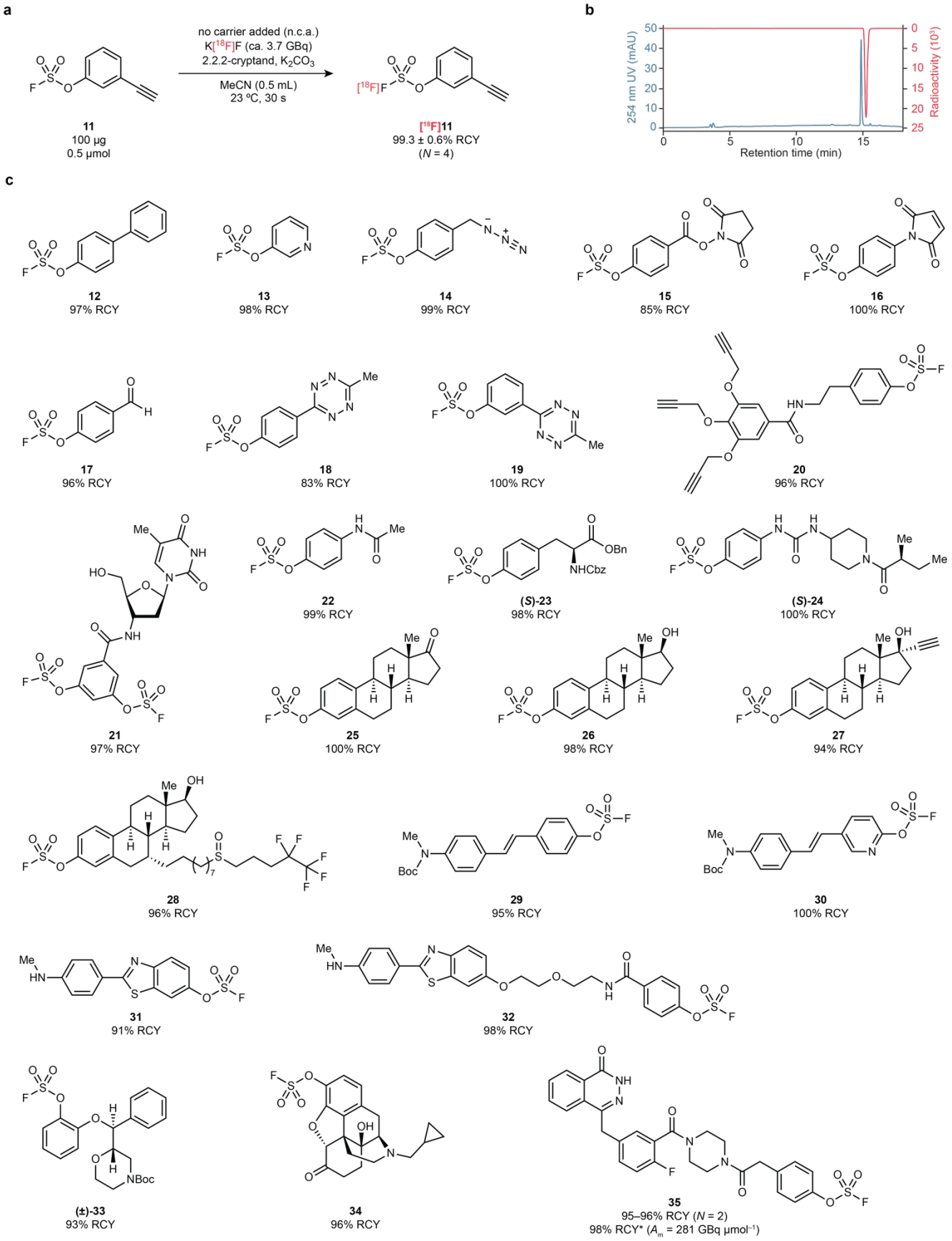
a
no carrier added (n.c.a.)
K[18F]F (ca. 3.7 GBq)
2.2.2-cryptand, K2CO3
MeCN (0.5 mL)
23 °C, 30 s
11
100 µg
0.5 µmol
[18F]11
99.3 ± 0.6% RCY
(N = 4)
b
254 nm UV (mAU)
Radioactivity (10³)
Retention time (min)
c
12
97% RCY
13
98% RCY
14
99% RCY
15
85% RCY
16
100% RCY
17
96% RCY
18
83% RCY
19
100% RCY
20
96% RCY
21
97% RCY
22
99% RCY
(S)-23
98% RCY
(S)-24
100% RCY
25
100% RCY
26
98% RCY
27
94% RCY
28
96% RCY
29
95% RCY
30
100% RCY
31
91% RCY
32
98% RCY
(±)-33
93% RCY
34
96% RCY
35
95–96% RCY (N = 2)
98% RCY* (Am = 281 GBq µmol⁻¹)

175

Fig. 3 | [^{18}F]SuFEx of aryl fluorosulfates. a, [^{18}F]SuFEx of 3-ethynylphenyl fluorosulfate (**11**). Conditions: Compound **11** (0.1 mg), K[^{18}F]F (ca. 3.7 GBq), [2.2.2]-cryptand, K_2CO_3, MeCN (0.5 mL), 23 ºC, 30 s. RCYs were determined by HPLC (*n* = 4) after the reaction crude being quenched by water (0.1 mL). **b**, Representative HPLC chromatograms of a reaction crude of [^{18}F]**11**, with 254 nm UV absorption (blue) and radioactivity (red) traces. **c**, Substrate scope of the [^{18}F]SuFEx reaction following the conditions described before (**a**). *Curie-scale synthesis of [^{18}F]**35**. Conditions: Compound **35** (0.1 mg, 17.2 nmol), K[^{18}F]F (ca. 34.6 GBq), [2.2.2]-cryptand, K_2CO_3, MeCN (10 mL), 23 ºC, 30 s. Me, methyl. Cbz, benzylcarbamate. Bn, benzyl.

Stability examination of aryl fluorosulfate radiopharmacophores in aqueous and biological milieu. To unravel the stability profile of aryl fluorosulfates in aqueous and biological milieu, we conducted a comprehensive examination of its propensity toward substitution and hydrolysis. Refluxing in the presence of aniline (bp 184 ºC) for 3 h induced no change of phenyl fluorosulfate (**1**, bp 180 ºC) (Supplementary **Fig. S2**). Incubating the same compound in aqueous HCl (1 mol L^{-1}) and 50% trifluoroacetic acid in DCM, respectively, for 24 h resulted in neglectable degradation (Supplementary **Fig. S6**). While being inert under physiological conditions (pH 7.4, 37 ºC) over a period of 1 week (**Fig. 4c**), **1** was hydrolyzed slowly in a pH 10 buffer (approximately 10% hydrolysis after 24 h, **Fig. 4a**) and rapidly by 0.025 mol L^{-1} aqueous sodium hydroxide ($t_{1/2}$ = 20 min). We then incubated **1** in pH 7.4 buffer in the presence of a series of nucleophilic or reductive amino acids and found that only lysine and glutathione (GSH) caused approximately 10% of **1** hydrolysis after 48-h (**Fig. 4b**).

Subsequently, the ^{18}F-labeled aryl fluorosulfate (*S*)-**24** was used to assess the *in vivo* stability of the $ArOSO_2$–F group. Upon injection into wild-type C57BL/6 mice via the intravenous (i.v.) route, [^{18}F]-(*S*)-**24** was found to be mainly enriched in liver where sEH is most abundantly expressed (**Fig. 4d**). Importantly, we did not detect apparent ^{18}F-associated signal in the bones — ^{18}F bone deposition[36] would indicate the release of [^{18}F]F^- from the aryl [^{18}F]fluorosulfate via an undesired substitution or

hydrolytic reaction. Similar *in vivo* stability was observed for the fulvestrant derivative [^{18}F]**28** (Supplementary **Fig. S62**). The absence of ^{18}F-associated signal in the bone provides strong evidence of the *in vivo* stability of [^{18}F]-(*S*)-**24** and [^{18}F]**28**, and suggests that aryl [^{18}F]fluorosulfates, in general, may indeed possess the required properties to be used for *in vivo* PET imaging.

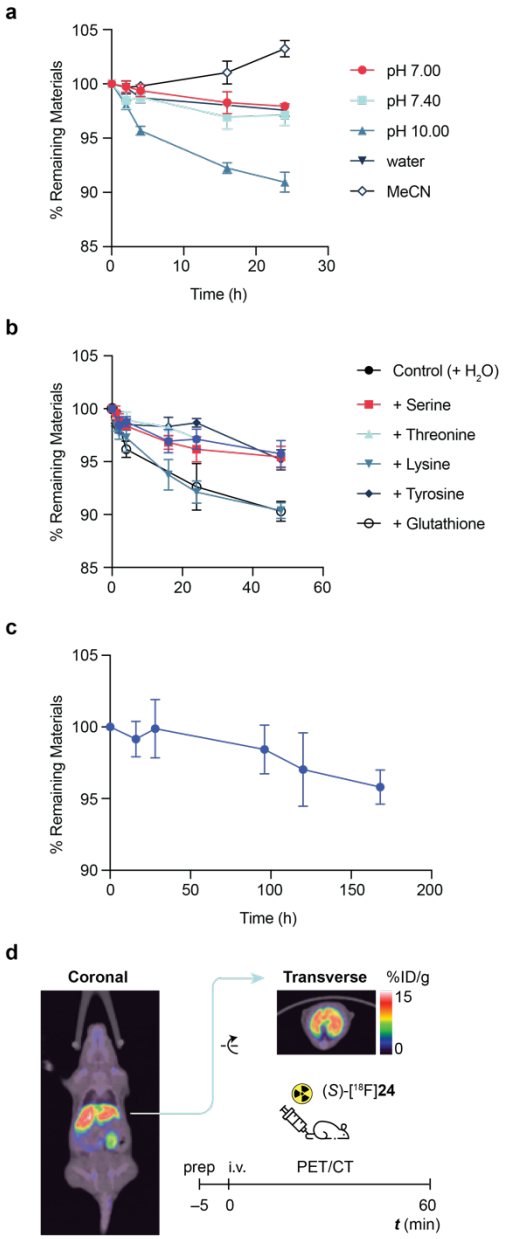

Fig. 4 | Stability characterization of aryl fluorosulfates *in vitro* and *in vivo*. a, Stability of **1** in phosphate buffers, water and MeCN at room temperature over a course of 24 h. Percentage of

remaining materials was quantified by HPLC (n = 3). **b,** Stability of **1** in pH 7.4 buffer in the presence of nucleophilic amino acids and reduced glutathione at room temperature (n = 3). **c,** Stability of **1** under physiological conditions, pH 7.4, 37 ºC (n = 3). **d,** PET images (60 min post-injection) of healthy mouse dosed by (*S*)-[^{18}F]**24** demonstrating its *in vivo* stability.

Structure-based design and application of a PARP-targeting aryl [^{18}F]fluorosulfate tracer To apply aryl [^{18}F]fluorosulfates to *in vivo* diagnostic PET imaging, we designed[37] a [^{18}F]fluorosulfate-functionalized analog of olaparib[38-40] (**35**) , an FDA-approved anti-cancer drug that targets tumor biomarker poly(ADP-ribose) polymerase 1 (PARP1), by extending the solvent-exposed site of olaparib with a pendent aryl fluorosulfate. Compound **35** maintained high binding affinity to PARP1 with a half maximal inhibitory concentration (IC_{50}) of 32.2 nM (**Fig. 5a**). When recombinant PARP1 was incubated with **35**, no formation of covalent adduct was detected by tandem mass spectrometry (LC-MS/MS), suggesting that compound **35** functions as a non-covalent PARP1 inhibitor. Importantly, **35** exhibited similar stability profile as olaparib in the serum of healthy human donors (**Fig. 5b**). Less than 25% of the small molecule was degraded after 3 h incubation, providing a useful time window for *in vivo* PET imaging.

A human breast cancer xenograft model was used to assess the applicability of the ^{18}F-labeled **35** for *in vivo* PET imaging. [^{18}F]**35** was i.v. injected into nude mice of subcutaneous human breast cancer xenograft established using MCF-7, a human breast cancer cell line with upregulated PARP1 expression. The intensive accumulation of the ^{18}F-labeled olaparib analog in tumors were clearly visualized with excellent target-to-background ratio after injection (**Fig. 5c**,**d**). In a competition experiment, excess olaparib was dosed before administration of [^{18}F]**35**, which blocked the accumulation of **35** in tumor, resulting in significant decrease in the ratio of % ID g^{-1} (injected dose per gram) of tumor-to-muscle from 2.02 ± 0.70 to 0.79 ± 0.04 (P < 0.05) (**Fig. 5c**,**e**). These

observations provide strong support for the specificity of this fluorosulfate-functionalized probe. Notably, in these experiments, we also detected significant ^{18}F-associated signals in the bone marrow that has abundant PARP1 expression[41,42].

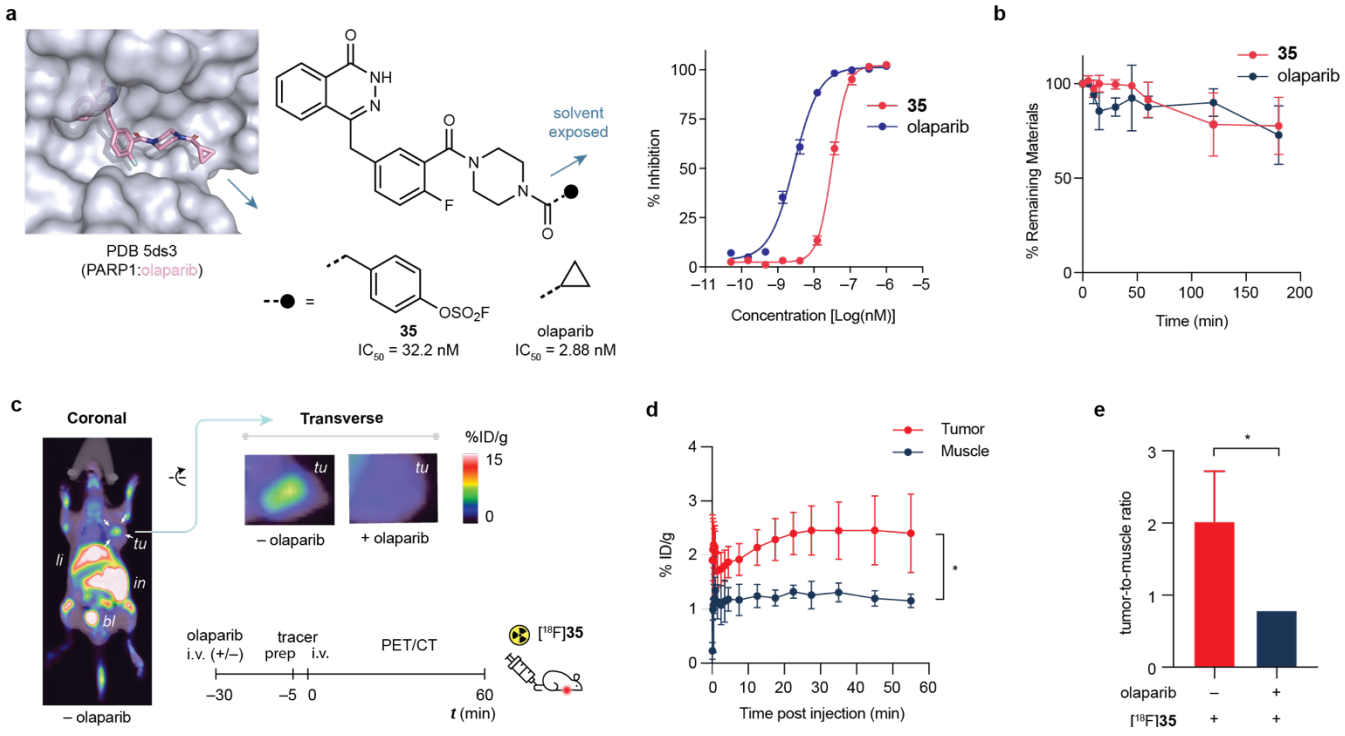

Fig. 5 | PET imaging in a tumor xenograft model using [^{18}F]35. **a**, Structure-based design of non-covalent PARP1 inhibitor **35** and its dose-response curve, olaparib as positive control. Error bars represent the mean plus standard deviation (SD, *n* = 3), IC_{50} = 32.2 nM. **b**, Serum stability of **35** is comparable to that of olaparib. **c**, Whole body coronal (left), and transverse (top-middle) PET/CT images of human MCF-7 bearing nude mice (transplanted under right shoulder, indicated by white arrows) acquired by performing a 55 min dynamic scan following [^{18}F]**35** administration. Transverse PET/CT image (top-right) of mice pre-treated by excess olaparib; No significant uptake of [^{18}F]**35** was observed at the tumor site. tu, tumor. li, liver. in, intestine. bl, bladder. **d**, Time plot of percentage of injected dose per gram (%ID g^{-1}) of tissue of interest. Error bars represent the mean plus standard

deviation (SD, n = 3). P-values were calculated by unpaired Student's t-test; *P < 0.05. **e**, Comparison of pre-treatment with either vehicle (n = 3) or 50 mg kg^{-1} or olaparib (n = 3) on the %ID g^{-1} ratio of tumor versus muscle (healthy tissue).

Discussion

Since its first introduction in 2014, aryl fluorosulfate-based SuFEx click chemistry has found a growing number of interesting applications in chemical biology. For example, the Kelly and Sharpless groups jointly discovered that a biphenyl-based aryl fluorosulfate inactivates intracellular lipid binding protein(s) through chemoselective SuFEx reaction with a Tyr residue in the ligand-binding site[43]. Likewise, by incorporating a fluorosulfate-equipped L-tyrosine, Wang and coworkers developed a proximity-enabled reactive PD-1 (programmed cell death protein-1) that reacts with a proximal histidine of PD-L1 selectively, enabling irreversible binding of PD-1 to only PD-L1 *in vitro* and *in vivo*[44]. Despite these pioneering studies that have demonstrated the potential of aryl fluorosulfates as covalent warheads for protein modifications, the reactivity-stability profile of S(VI)-F in a biological milieu remains elusive. Anyone that plans to use aryl fluorosulfates for biological applications should be cautious to assume their propensity to undergo any covalent transformations under physiological conditions. As a matter of fact, compared to the newly developed iminosulfur oxydifluorides[45,46], aryl fluorosulfates are uniquely inert to disordered nucleophiles in bulk water due to its neglectable net dipole. Works by others[47-49], and our own labs[43,50] have partially unraveled the stringent requirements for its activation. Only with the orientation of an aryl fluorosulfate and its reactive partner immobilized to just right, like a freeze-frame, by local electrostatic effects and an organized hydrogen bonding network, covalent capture would take place at the time scale of small molecule binding. Neither elongated contact nor perturbed nucleophile reactivity is dispensable. Accordingly, a protein, upon denaturing and losing its tertiary structure, immediately loses its reactivity with an aryl fluorosulfate-functionalized molecule that

readily reacts with the same protein under native conditions[37,43]. This is the exact design principle upon which Kelly, Sharpless and Wang's work was built.

On the other hand, the above covalent capture examples reflect only a tip of the reactivity landscape of aryl fluorosulfates. In a few extreme cases we have encountered, yet contrary to the biased common sense that acid halide is labile, aryl fluorosulfates stay intact in refluxing aniline (184 ºC), aqueous solutions (**Fig. 4**) and even in the presence of an entire proteome[43]. The realization of the narrow reactivity-window has, thence, led to the scenario of taking advantage of the overlooked stability. As proof-of-principle, we have developed non-covalent inhibitors ((*S*)-**24**, **28**) by late-stage fluorosulfonylation of phenolic drugs[24] and bioisosteric replacement of trifluoromethoxy group[25], respectively, with improved potency and metabolic stability and the *in vivo* inertness of these compounds has been confirmed by pharmacokinetic evaluations.

Here, by exploiting the intrinsic chemical inertness of aryl fluorosulfate, we have developed aryl [^{18}F]fluorosulfate-based radiotracers for *in vivo* PET imaging in wt mice and in a xenograft tumor model. We discovered that fluoride anions circumvented the high kinetic barrier of a typical SuFEx reaction associated with amine or alcohol nucleophiles—the extraneous fluoride anion *per se* compensates the stringent requirements in the latter scenarios for the stabilization or solvation of the departing fluoride from an S^{VI}–F site. Driven by this mechanistic rationale, we have successfully developed an ultrafast [^{18}F]SuFEx process to incorporate ^{18}F into aryl fluorosulfates as new radiotracers that, in the meantime, possess sufficient stability to be used for *in vivo* imaging with negligible drawbacks of hydrolysis and covalent bond formation.

The most unique feature of [^{18}F]SuFEx is its efficiency and fidelity without sacrificing the probe's stability. The traditional radiosynthesis of an ^{18}F-tagged *N*-hydroxysuccinimide ester (NHS) requires sequential S_NAr, saponification, and esterification, and a 20-min HPLC purification[51]. By contrast, [^{18}F]SuFEx fulfills ^{18}F installation and purification at room temperature within 2 min ([^{18}F]**15**). To our knowledge, [^{18}F]SuFEx represents the fastest ^{18}F-incorporation process to date.

The mild exchange condition and chemical orthogonality of SuFEx also rendered a much broader substrate scope than the previously known radiolabeling protocols (**Fig. 3**). Thus, the radiolabeling could be accomplished in the final step of the tracer synthesis with significantly less activity going futile. The chemical inertness of aryl fluorosulfates also offers much flexibility in planning the "cold" precursor preparation such that the fluorosulfate handle may be installed in either early (e.g. **35** and fluorosulfonylated peptides[25]) or late stages (e.g. **33**, **34**) in a synthetic scheme.

In short, aryl [^{18}F]fluorosulfates complement the current C–^{18}F toolkit by unlocking an uncharted radiochemical space. We envisage that it is possible to rationally design additional aryl [^{18}F]fluorosulfate-containing radiotracers to probe proteins beyond the ones described here, such as radiotracers for targeting the central nervous system.

Acknowledgements

This work is supported by the U.S. National Institutes of Health (R01GM117145 to K.B.S., R01GM093282 to P.W., and R01GM100934 to L.N.), the U.S. National Science Foundation (CHE-1610987 to K.B.S.), the National Natural Science Foundation of China (21977070 to G.Y.), and ShanghaiTech University startup fund (G.Y.). Q.Z. is an Ellen Browning Scripps Graduate Fellow. We thank Huayi Isotopes Co. (Changshu, Jiangsu Province, China) for access of cyclotron and PET-CT, Dr. Dee-Hua Huang (Scripps Research NMR Facility) for assistance on TDST-NMR experiments, Prof. Jin-Quan Yu (Scripps Research) for access of glovebox and GC-EI-MS, Dr. Yongxuan Su (UC San Diego) for assistance on APCI-MS. We are grateful to Prof. Jiajia Dong (Shanghai Institute of Organic Chemistry) for helpful discussions.

Author contributions: K.B.S., P.W., H.W. and Q.Z. conceived the work. Q.Z., and H.W. designed and executed TDST-NMR study. Q.Z. performed chemical syntheses and characterizations. Q.Z., H.Xu and P.W. designed bioassays. Q.Z. and H.Xu designed and executed radiosynthesis and PET imaging.

N.W., and H.Xiong synthesized and assayed PARP1 inhibitors. W.-G.H.D., and L.N. performed computational study. Q.Z., P.W., and K.B.S. wrote the manuscript; all authors edited the manuscript.

Data and materials availability: Experimental procedures for chemical and radiosynthesis, ^{1}H-NMR, ^{13}C-NMR, ^{19}F-NMR, ^{19}F-TDST-NMR spectra, analytical HPLC radioactivity and UV chromatograms, PET-CT images, immunohistochemistry, and DFT calculations are available in the supplementary materials.

Reference

1 Fowler, J. S. & Wolf, A. P. Working against time: Rapid radiotracer synthesis and imaging the human brain. *Acc. Chem. Res.* **30**, 181-188 (1997).

2 Phelps, M. E. Positron emission tomography provides molecular imaging of biological processes. *Proc. Natl. Acad. Sci. USA* **97**, 9226-9233 (2000).

3 Gambhir, S. S. Molecular imaging of cancer with positron emission tomography. *Nat. Rev. Cancer* **2**, 683-693 (2002).

4 Tsien, R. Y. Imagining imaging's future. *Nat. Rev. Mol. Cell Bio.*, SS16-SS21 (2003).

5 Willmann, J. K., van Bruggen, N., Dinkelborg, L. M. & Gambhir, S. S. Molecular imaging in drug development. *Nat. Rev. Drug Discov.* **7**, 591-607 (2008).

6 Ametamey, S. M., Honer, M. & Schubiger, P. A. Molecular imaging with PET. *Chem. Rev.* **108**, 1501-1516 (2008).

7 Cai, L. S., Lu, S. Y. & Pike, V. W. Chemistry with [F-18]fluoride ion. *Eur. J. Org. Chem.*, 2853-2873 (2008).

8 Tredwell, M. & Gouverneur, V. 18F Labeling of Arenes. *Angew. Chem. Int. Ed.* **51**, 11426-11437 (2012).

9 Brooks, A. F., Topczewski, J. J., Ichiishi, N., Sanford, M. S. & Scott, P. J. H. Late-stage [F-18]fluorination: new solutions to old problems. *Chem. Sci.* **5**, 4545-4553 (2014).

10 Liang, S. H. & Vasdev, N. C(sp(3))-F-18 Bond Formation by Transition-Metal-Based [F-18]Fluorination. *Angew. Chem. Int. Ed.* **53**, 11416-11418 (2014).

11 Preshlock, S., Tredwell, M. & Gouverneur, V. F-18-Labeling of Arenes and Heteroarenes for Applications in Positron Emission Tomography. *Chem. Rev.* **116**, 719-766 (2016).

12 Lee, E. *et al.* A Fluoride-Derived Electrophilic Late-Stage Fluorination Reagent for PET Imaging. *Science* **334**, 639-642 (2011).

13 Huiban, M. *et al.* A broadly applicable [F-18]trifluoromethylation of aryl and heteroaryl iodides for PET imaging. *Nat. Chem.* **5**, 941-944 (2013).

14 Graham, T. J. A., Lambert, R. F., Ploessl, K., Kung, H. F. & Doyle, A. G. Enantioselective Radiosynthesis of Positron Emission Tomography (PET) Tracers Containing [F-18]Fluorohydrins. *J. Am. Chem. Soc.* **136**, 5291-5294 (2014).

15 Rotstein, B. H., Stephenson, N. A., Vasdev, N. & Liang, S. H. Spirocyclic hypervalent iodine(III)-mediated radiofluorination of non-activated and hindered aromatics. *Nat. Commun.* **5**, 4365 (2014).

16 Sergeev, M. E., Morgia, F., Lazari, M., Wang, C. & van Dam, R. M. Titania-Catalyzed Radiofluorination of Tosylated Precursors in Highly Aqueous Medium. *J. Am. Chem. Soc.* **137**, 5686-5694 (2015).

17 Neumann, C. N., Hooker, J. M. & Ritter, T. Concerted nucleophilic aromatic substitution with F-19(-) and F-18(-). *Nature* **538**, 369-373 (2016).

18 Levin, M. D. *et al.* A catalytic fluoride-rebound mechanism for C(sp(3))-CF3 bond formation. *Science* **356**, 1272-1275 (2017).

19 Chen, W. *et al.* Direct arene C-H fluorination with (18)F(-) via organic photoredox catalysis. *Science* **364**, 1170-1174 (2019).

20 Ido, T. *et al.* Labeled 2-Deoxy-D-Glucose Analogs - F-18-Labeled 2-Deoxy-2-Fluoro-D-Glucose, 2-Deoxy-2-Fluoro-D-Mannose and C-14-2-Deoxy-2-Fluoro-D-Glucose. *J. Labelled Compd. Rad.* **14**, 175-183 (1978).

21 Campbell, M. G. *et al.* Bridging the gaps in F-18 PET tracer development. *Nat. Chem.* **9**, 1-3 (2017).

22 Kolb, H. C., Finn, M. G. & Sharpless, K. B. Click chemistry: Diverse chemical function from a few good reactions. *Angew. Chem. Int. Ed.* **40**, 2004-2021 (2001).

23 Dong, J., Sharpless, K. B., Kelly, J. W. & Chen, W. Sulfur (VI) fluoride compounds and methods for the preparation thereof. US patent 10,117,840 (2018).

24 Dong, J. J., Krasnova, L., Finn, M. G. & Sharpless, K. B. Sulfur(VI) Fluoride Exchange (SuFEx): Another Good Reaction for Click Chemistry. *Angew. Chem. Int. Ed.* **53**, 9430-9448 (2014).

25 Chen, W. *et al.* Synthesis of Sulfotyrosine-Containing Peptides by Incorporating Fluorosulfated Tyrosine Using an Fmoc-Based Solid-Phase Strategy. *Angew. Chem. Int. Ed.* **55**, 1835-1838 (2016).

26 Brown, D. G. & Boström, J. Analysis of Past and Present Synthetic Methodologies on Medicinal Chemistry: Where Have All the New Reactions Gone? *J. Med. Chem.* **59**, 4443-4458 (2016).

27 Bernard-Gauthier, V. *et al.* 18F-labeled silicon-based fluoride acceptors: potential opportunities for novel positron emitting radiopharmaceuticals. *BioMed Res. Int.* **2014**, 454503 (2014).

28 Taitelbaum, H., Weiss, G. H. & Spencer, R. G. S. Optimization of Magnetization-Transfer Experiments for Kinetic Rate Measurements. *NMR Biomed.* **7**, 287-292 (1994).

29 Gao, B. *et al.* Bifluoride-catalysed sulfur(VI) fluoride exchange reaction for the synthesis of polysulfates and polysulfonates. *Nat. Chem.* **9**, 1083-1088 (2017).

30 Coenen, H. H. *et al.* Consensus nomenclature rules for radiopharmaceutical chemistry - Setting the record straight. *Nucl. Med. Biol.* **55**, V-Xi (2017).

31 Meyer, J. P., Adumeau, P., Lewis, J. S. & Zeglis, B. M. Click Chemistry and Radiochemistry: The First 10 Years. *Bioconjugate Chem.* **27**, 2791-2807 (2016).

32 Wong, D. F. *et al.* In vivo imaging of amyloid deposition in Alzheimer disease using the radioligand 18F-AV-45 (florbetapir [corrected] F 18). *J. Nucl. Med.* **51**, 913-920 (2010).

33 Zhang, W. *et al.* F-18 Polyethyleneglycol stilbenes as PET imaging agents targeting Aβ aggregates in the brain. *Nucl. Med. Biol.* **32**, 799-809 (2005).

34 Klunk, W. E. *et al.* Imaging brain amyloid in Alzheimer's disease with Pittsburgh Compound-B. *Ann. Neurol.* **55**, 306-319 (2004).

35 Rami-Mark, C. *et al.* [18F]FMeNER-D2: Reliable fully-automated synthesis for visualization of the norepinephrine transporter. *Nucl. Med. Biol.* **40**, 1049-1054 (2013).

36 Grant, F. D. *et al.* Skeletal PET with 18F-fluoride: applying new technology to an old tracer. *J. Nucl. Med.* **49**, 68-78 (2008).

37 Jones, L. H. & Kelly, J. W. Structure-based design and analysis of SuFEx chemical probes. *RSC Med. Chem.* **11**, 10-17 (2020).

38 Dawicki-McKenna, J. M. *et al.* PARP-1 Activation Requires Local Unfolding of an Autoinhibitory Domain. *Mol. Cell* **60**, 755-768 (2015).

39 Carney, B. *et al.* Non-invasive PET Imaging of PARP1 Expression in Glioblastoma Models. *Mol. Imaging Biol.* **18**, 386-392 (2016).

40 Carney, B. *et al.* Target engagement imaging of PARP inhibitors in small-cell lung cancer. *Nat. Commun.* **9**, 176 (2018).

41 Uhlen, M. *et al.* Proteomics. Tissue-based map of the human proteome. *Science* **347**, 1260419 (2015).

42 Human Protein Atlas. *PARP1*, <https://www.proteinatlas.org/ENSG00000143799-PARP1/tissue> (n.d.).

43 Chen, W. *et al.* Arylfluorosulfates Inactivate Intracellular Lipid Binding Protein(s) through Chemoselective SuFEx Reaction with a Binding Site Tyr Residue. *J. Am. Chem. Soc.* **138**, 7353-7364 (2016).

44 Li, Q. *et al.* Developing Covalent Protein Drugs via Proximity-Enabled Reactive Therapeutics. *Cell* **182**, 85-97 (2020).

45 Li, S., Wu, P., Moses, J. E. & Sharpless, K. B. Multidimensional SuFEx Click Chemistry: Sequential Sulfur(VI) Fluoride Exchange Connections of Diverse Modules Launched From An SOF4 Hub. *Angew. Chem. Int. Ed.* **56**, 2903-2908 (2017).

46 Kitamura, S. *et al.* Sulfur(VI) Fluoride Exchange (SuFEx)-Enabled High-Throughput Medicinal Chemistry. *J. Am. Chem. Soc.* **142**, 10899-10904 (2020).

47 Jones, L. H. Emerging Utility of Fluorosulfate Chemical Probes. *ACS Med. Chem. Lett.* **9**, 584-586 (2018).

48 Fadeyi, O. O. *et al.* Covalent Enzyme Inhibition through Fluorosulfate Modification of a Noncatalytic Serine Residue. *ACS Chem. Biol.* **12**, 2015-2020 (2017).

49 Wang, N. *et al.* Genetically Encoding Fluorosulfate-l-tyrosine To React with Lysine, Histidine, and Tyrosine via SuFEx in Proteins in Vivo. *J. Am. Chem. Soc.* **140**, 4995-4999 (2018).

50 Mortenson, D. E. *et al.* "Inverse Drug Discovery" Strategy To Identify Proteins That Are Targeted by Latent Electrophiles As Exemplified by Aryl Fluorosulfates. *J. Am. Chem. Soc.* **140**, 200-210 (2018).

51 Shao, X. in *Radiopharmaceuticals for Positron Emission Tomography* Vol. 1 *Radiochemical Syntheses* (eds Peter J. H. Scott & Brian G. Hockley) Ch. 9, 81-85 (Wiley, 2012).